Journal of Materials Chemistry A

Tuning self-healing properties of stiff, ion-conductive polymers

Journal:	*Journal of Materials Chemistry A*
Manuscript ID	TA-ART-11-2018-011353.R1
Article Type:	Paper
Date Submitted by the Author:	08-Feb-2019
Complete List of Authors:	Qin, Jiaxu; University of Washington, Molecular Engineering & Science Institute Lin, Francis; University of Washington, Department of Chemistry Hubble, Dion; University of Washington, Molecular Engineering & Sciences Institute Wang, Yujia; University of Washington, Chemistry Li, Yun; University of Washington, Materials Science and Engineering Murphy, Ian; University of Washington, Department of Chemistry Jang, Sei-Hum; University of Washington, Department of Chemistry Yang, Jihui; University of Washington, Materials Science and Engineering Jen, Alex; University of Washington, Materials Science and Engineering; University of Washington, Chemistry

Journal Name

ARTICLE

Tuning self-healing properties of stiff, ion-conductive polymers

Jiaxu Qin[a], Francis Lin[b], Dion Hubble[a], Yujia Wang[b], Yun Li[c], Ian A. Murphy[b], Sei-Hum Jang[bc], Jihui Yang[c] and Alex K.-Y. Jen[*abcd]

Received 00th January 20xx,
Accepted 00th January 20xx

DOI: 10.1039/x0xx00000x

www.rsc.org/

Although various self-healing polymers have been developed, individual designs are generally limited to a narrow range of possible mechanical properties and self-healing temperatures, as it's challenging to tune these characteristics over a wide range without re-engineering molecular structure entirely. Here, a strategy to decouple self-healing and mechanical properties from the covalent structure of supramolecular polymers, and a novel material system developed using this strategy, which is based on non-covalent π–π interactions between naphthalene diimide (NDI) and pyrene (Py) derivatives are reported. Through targeted, stoichiometric addition of small model compounds, both binding strength and overall density of crosslinking interactions are modulated successfully. This strategy allows us to tune both self-healing temperature (30-60 °C) and Young's modulus (63-250 MPa) of our materials over a wide range, without changing the structure of polymer components. Our self-healing polymer system also displays good solid-state ionic conductivity (> 10^{-5} S/cm at room temperature) after doping with Li(G4)TFSI, and could function as cathode binder in lithium-sulfur battery to give high discharge capacity of 1109 mAh/g at C/5. The rational design strategy and resultant material platform demonstrated represent a first step towards a class of highly tunable self-healing polymers, for electrochemical devices.

1. Introduction

Materials exhibiting self-healing behavior are very desirable for electrochemical devices across a number of emerging applications.[1–5] For example, artificial skin, flexible electronics, and rechargeable batteries may all experience strain-induced cracking during normal operation due to mechanical activity, resulting in loss of conductive pathways and reduction in device performance.[6–9] Introduction of self-healing feature into such devices can help reform these pathways after breakage, with associated recovery of performance.[10–12] Organic polymers are a natural choice of platform to introduce self-healing behavior into electrochemical devices, given their combined good processability, mechanical flexibility, and inexhaustible variety of molecular structures.[13–15]

In general, self-healing in polymers results from the reformation of broken molecular linkages between polymer chains. Self-healing polymers are usually crosslinked *via* reversible noncovalent interactions[16–23] or dynamic covalent interactions,[19,24,25] with the resulting macro-scale properties (such as self-healing temperature and tensile modulus) being determined by the overall strength and density of such crosslinking interactions. These interactions are, in turn, tightly coupled to the spatial structure of the polymers at the molecular level. Most previous studies take the logical approach of altering macro-scale properties through re-engineering of molecular structure, including modification of polymer backbones[14,26] and side-chains,[21,22] copolymerization,[22,23] and hybridization of polymers and inorganic materials.[24,25] Each new target application requires an entirely new polymer design, which makes most individual materials only suitable for a small group of applications, due to the narrow range of properties achievable for a particular structure.

For instance, an effective battery binder would likely require a vastly different tensile modulus than a biosensor,[32–35] as well as the ability to self-heal under a wide range of operating temperatures,[36,37] as opposed to the narrow range of temperatures associated with the human body.[38,39] Given the tight coupling of molecular structure to properties,[40] common sense dictates that these two applications would thus require polymers with vastly different designs. However, the design, synthesis, and optimization of entirely new organic materials is a challenging and time-consuming endeavor, with the resulting new materials suffering from their own narrow range of usability. While this design-property feedback loop has encouraged development of a wide range of creative molecular structures, it has also limited the ability of the field to respond to new challenges on a timescale that allows widespread utilization of self-healing polymers in real devices.

In contrast to the traditional focus on spatial hierarchy of polymers, we report here a strategy to decouple crosslinking behavior, including binding strength and density, from the molecular structure of self-healing systems. We introduce a supramolecular polymer system in which polymer PENDI - containing naphthalenediimide (NDI) side chains - is physically crosslinked by trivalent linkers triPy -containing pyrene (Py) units *via* reversible face-to-face quadrupole-quadrupole interactions between NDI and

[a] *Molecular Engineering & Science Institute, University of Washington, Seattle, Washington, 98195, United States.*
[b] *Department of Chemistry, University of Washington, Seattle, Washington, 98195, United States.*
[c] *Department of Materials Science and Engineering, University of Washington, Seattle, Washington, 98195, United States.*
[d] *Department of Chemistry, and Department of Materials Science & Engineering, City University of Hong Kong, Kowloon 999077, Hong Kong.*

†Electronic Supplementary Information (ESI) available: Experimental details of UV-vis spectra; TGA and DSC data; AFM test, self-healing, and uniaxial tensile tests. See DOI: 10.1039/x0xx00000x

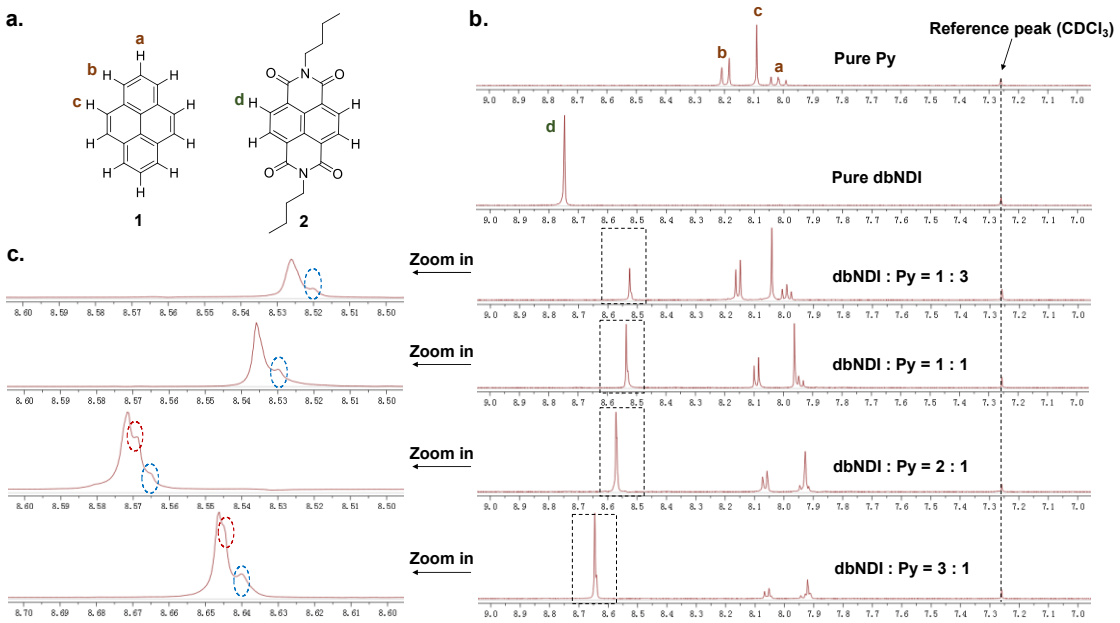

Fig. 1 NMR spectra of dbNDI and Py mixtures with different molar ratio in chloroform-*d*. (a) The two model compounds Py (**1**) and dbNDI (**2**). (b) The aromatic ring proton signals of model compounds. (c) The signal peak change of proton **d** in dbNDI.

Py. By adding small molecules which also contain these functionalities, we are able to demonstrate modulation of different binding modes between NDI and Py, which possess different strength, *via* stoichiometry control, as well as modulation of the density of interactions between NDI and Py units on polymer chains (as opposed to interactions with the free, small molecules). This allows us to develop a series of self-healing materials in which both crosslinking density and binding strength are tunable without modifying polymer structure or composition.

Consequently, the mechanical performance and self-healing temperature of our system can be modulated within a wide range. Our material system not only possesses high stiffness (Young's modulus > 69 MPa) and good stretchability (>100% strain), but also good solid-state ionic conductivity when doped with Li(G4)TFSI (> 10^{-5} S/cm at room temperature), enabling it to be integrated into electrochemically-active systems without breaking conductive pathways. Thus, we provide a novel design strategy to decouple macroscopic properties from polymer structure in self-healing materials, widening the potential applicability window of individual structural motifs, which shows promise for use in future electrochemical devices.

2. Results and Discussion

2.1 Characterization of the Intermolecular Interactions

To understand the nature of intermolecular interactions between NDI and Py derivatives, model compounds dibutyl-NDI (dbNDI) and pyrene (Py) were studied. The formation of face-to-face charge transfer (CT) complexes resulting from intermolecular quadrupole-quadrupole interactions between electron-deficient NDI derivatives and electron-rich Py is well described in the literature.[41–44] The formation of this complex was confirmed by stoichiometrically mixing Py and dbNDI in dichloromethane. A new absorbance peak emerged at 500 nm wavelength (see Supporting Information, **Fig. S1**), implying the formation of a 1:1 CT complex between Py and dbNDI. Interestingly, when the molar ratio between dbNDI and Py was changed while maintaining the same overall molar concentration, we found that an additional characteristic absorbance peak emerged at 514 nm when dbNDI was in excess (**Fig. S2**). This absorbance peak reached a maximum at a dbNDI:Py ratio of 2:1, suggesting a new complex structure of this stoichiometry.

Concurrently, the formation of complexes was observed with different binding modes in the H^1 NMR spectra of dbNDI and Py mixtures. The aromatic ring proton signals are highlighted in **Fig. 1**. In pure dbNDI, proton **d** was observed to appear as a peak at 8.75 ppm. After mixing dbNDI and Py in a ratio of 1:3, the position of proton **d** shifted upfield to around 8.53 ppm, presumably due to the shielding effect of Py *via* π–π interaction. Decreasing the ratio to 1:1 effected only a slight change on the position of this peak; however, further decreasing the amount of Py resulted in a noticeable shift back downfield. This behavior suggests the formation of a new complex in which proton **d** is shielded less significantly by electron density on Py.

Besides simply shifting positions, the signal of proton **d** on the dbNDI ring also changed structure with varying molar ratio: in pure dbNDI, proton **d** possesses a single peak, whereas a small additional peak appeared upon the introduction of an excess of Py (dbNDI:Py = 1:3), implying the formation of long-lived complex which breaks the symmetry of aromatic protons on dbNDI. This new peak became more apparent when the ratio was increased to dbNDI:Py = 1:1. Upon increasing the concentration of dbNDI even further such that dbNDI is in excess (dbNDI:Py = 2:1 and 3:1), an additional new peak appeared, indicating yet another break in symmetry and implying the

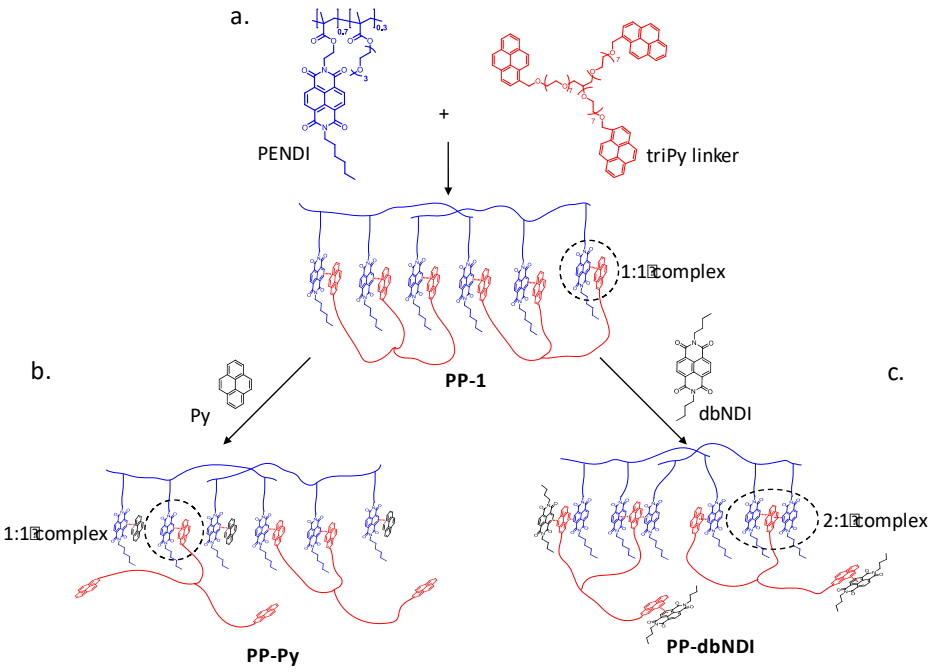

Fig. 2 Design concept for PP supramolecular polymers and tuning of binding modes. a) Structural design of PP-1, utilizing triPy to crosslink PENDI with an equal molar ratio of NDI side chains and Py units. b) Structure of PP-Py, with 1:1 complexes favored by occupying half of NDI side chains of PENDI with free Py. c) Structure of PP-dbNDI, with 2:1 complexes favored by the addition of model compound dbNDI.

formation of different type of complex. The synchronicity of both NMR and UV-Vis data suggests two types of binding modes in this system corresponding to 1:1 and 2:1 ratios of dbNDI:Py, as well as modulation of the dominant binding mode through stoichiometry control.

The average free energy of complexation of these two interaction modes was further estimated by using the UV-Vis dilution method in dichloromethane (**Fig. S3**, **Table S1**).[39,40] We found that the free energy of complexation of the 1:1 complex (-8.19 kJ/mol) is significantly weaker than that of the 2:1 complex (-16.49 kJ/mol).

The large difference in binding energy of these complexes, in addition to the tunability of NDI/Py interactions based on stoichiometry, makes this combination an intriguing choice for crosslinking units in a self-healing polymer. Here we note a few important points: first, in most self-healing polymers, changing the concentration of crosslinking groups only results in modulation of crosslinking density.[24,26] Interestingly, in our system, it appears that changing the ratio between NDI and Py not only can tune the crosslinking density, but also fundamentally change the predominant binding mode, and therefore the binding energy. This means that, in principle, we can tune polymer properties over a wide range by simply changing the ratio between NDI unit and Py unit. Second, when adjusting this ratio, NDI and Py units do not need to come from the polymer side chains. Instead, they can be added in the form as small molecule dopants. Such additives would encourage, and participate in, the formation of one complex over another without altering the number of crosslinking units available. Thus, we can dope small molecules into the polymer to change both binding mode and crosslinking density, providing a general and rational molecular design strategy to control material properties over a wide-range without having to change the structure of the polymer itself.

2.2 Design of Self-Healing Polymers

The aforementioned tunable interaction modes between NDI and Py derivatives were used as the basis of self-healing in our PENDI-triPy (PP) supramolecular polymer. Specifically, PP utilizes triPy linker to reversibly crosslink PENDI *via* π–π interactions between NDI side chains and Py units (**Fig. 2**). Each feature of this system is selected rationally: the rigid methacrylate backbone of PENDI is expected to provide the PP system with a high Young's modulus, while the oligo(ethylene glycol) (OEG) chains present in both PENDI and triPy lend chain flexibility, which ultimately facilitates self-healing efficiency. The tunable and versatile binding modes between Py units and NDI side chains provide a "molecular handle" with which to adjust polymer properties. Consequently, the binding strength and crosslinking density of the supramolecular polymer are determined by the dominant binding modes, which are modulated by the relative ratio between NDI and Py.

Polymer PENDI (M_n = 102.4 KDa, PDI = 1.30) and triPy linker were synthesized. Three PP composites, corresponding to different model compound doping strategies, were designed using PENDI and triPy. As depicted in **Fig. 2a**, PP-1 composite consists of PENDI and triPy with a molar ratio between NDI side-chains and Py units of 1:1. Based on our study of molar ratio control in the substituent compounds, the crosslinking mode should be predominantly 1:1 binding complexes. To modulate the crosslinking density without changing

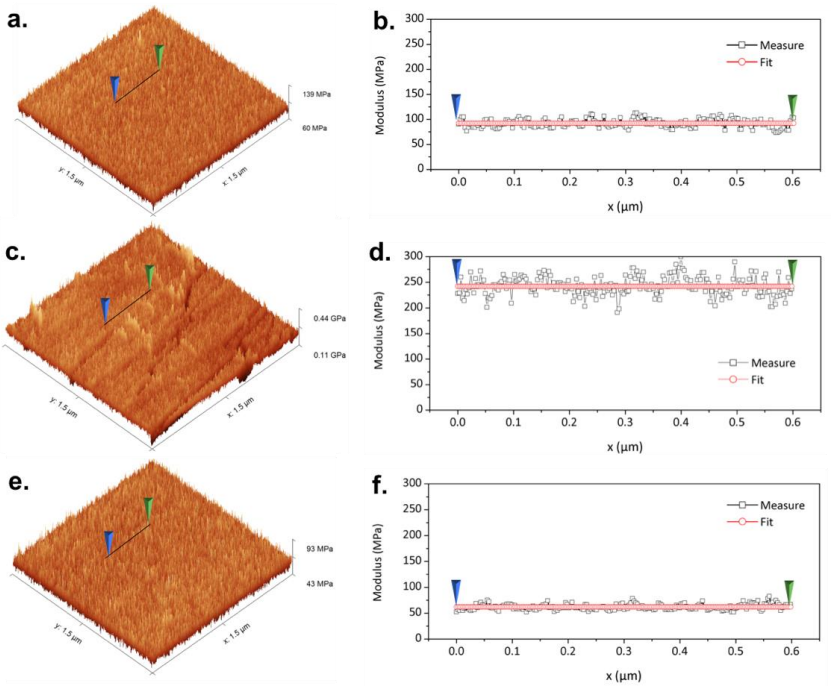

Fig. 3 3D Young's modulus maps generated *via* AFM test, along with the measured and fitted average (black and red lines, respectively) Young's moduli of selected linear area in PP-1 (a and b), PP-dbNDI (c and d), and PP-Py (e and f).

polymer structure, an additional half molar equivalent of small molecule additive Py was added relative to total NDI side chains present, forming PP-Py composite (**Fig. 2b**). Then PP-Py composite should possess the 1:1 binding mode almost exclusively, but with a lower crosslinking density than PP-1, as half of the NDI side-chains are tied up in non-crosslinking interactions with free Py molecules. Similarly, by adding half molar equivalent of additive dbNDI relative to total Py units present into PP-1, we created the PP-dbNDI composites (**Fig. 2c**). Due to the stacking interaction between small molecule dbNDI and Py units, the amount of free NDI side chains will be higher than Py units. The excessive NDI moieties present in this system ensures that the majority of Py units will be bound in the stronger 2:1 mode, without significantly changing the overall density of total crosslinks formed. It should be noticed that the intuitively easiest way to change the NDI/Py ratio in our system would be to change the mix ratio between PENDI and triPy. However, because both of these materials contain polymeric/oligomeric structures in addition to NDI/Py functionality, changing the mix ratio will also change the spatial structure of the resulting PP system, which affects mechanical property significantly. For example, if we double the content of triPy, the mechanical strength of the resulting PP polymer system will dramatically decrease due to the lack of long-chain rigid polymer PENDI and the abundance of liquid-like triPy. Therefore, it is not only sacrificing the mechanical property, but also difficult to determine how much of the observed change in properties can be attributed to reversible interaction, as opposed to backbone content.

2.3 Mechanical Properties of Self-Healing Polymers

The Young's moduli of these polymer composites were first probed *via* AFM to investigate the effect of different binding modes on mechanical properties (**Fig. 3**). The 3D Young's modulus maps reveal that PP-1 possesses a large average modulus of 92 MPa. We hypothesize that this is because PENDI, with a high glass transition temperature (T_g = 93°C, **Fig. S5**) and Young's modulus of 104 MPa (**Fig. S6**), provides a high baseline stiffness owing to its rigid methacrylate backbone. PP-Py possesses a Young's modulus that is slightly lower than PP-1 at 62 MPa. We attribute this to the lower crosslinking density in PP-Py, due to the existence of model compound Py which occupies NDI side-chains. On the other hand, the Young's modulus of PP-dbNDI (241 MPa) is much higher than that of PP-1. This drastic increase can be explained by a shift in predominant interaction mode from the 1:1 complex to the much stronger 2:1 complex. Accordingly, the Young's modulus increases significantly due to the higher energy required to break the CT complex. Meanwhile, the stronger binding strength also results in a rougher surface of PP-dbNDI (**Fig S7**). Notably, all composites exhibit Young's moduli far greater than the majority of self-healing materials in literature (<10 MPa).[47–50] This is because most of the previously reported self-healing polymer designs, including soft gels, elastomers, and even hybrid organic-inorganic composites, typically sacrifice stiffness to achieve self-healing properties. The high stiffness of our design should help maintain the physical integrity of materials which suffer from volume expansion or deformation damage.

The mechanical properties of the polymers were further studied by uniaxial tensile tests. As shown in **Fig. 4a**, the measured moduli (116 MPa for PP-1, 70 MPa for PP-Py, 219 MPa for PP-dbNDI) generally agree with the AFM test results. Tensile test results also reveal that the PP systems possess high maximum tensile stress (>2.1 MPa), especially for dbNDI (3.48 MPa). To visually demonstrate this resilience, constant stress of about 1 MPa was applied to a PP-1 film for 1 h at room temperature, resulting in no obvious deformation (**Fig. 4b, Fig S8**). This high stiffness and high yield point suggest that the polymer is highly resistant to deformation and cracking, which can

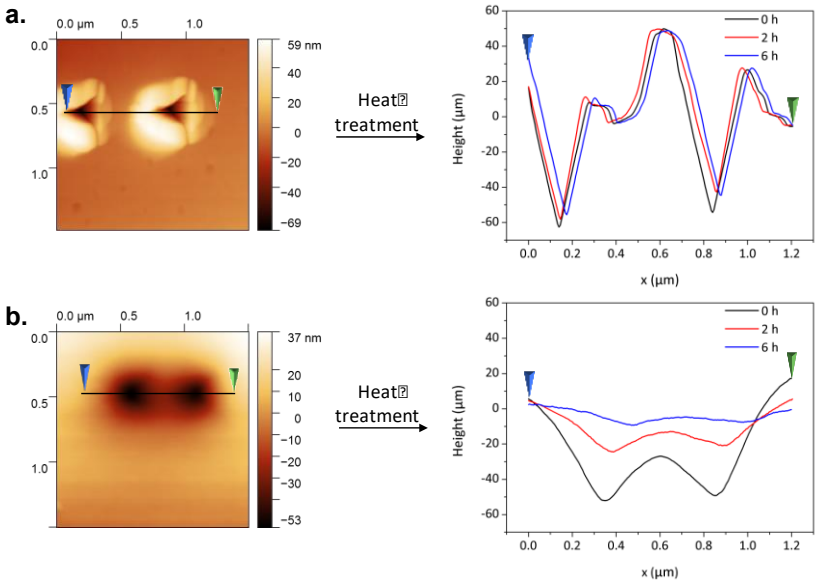

Fig. 5 AFM height profiles of PENDI (a) and PP-1 (b) films after being punched by AFM tip followed by heat treatment at 40 °C for different times.

be helpful to maintain the physical integrity of mechanically-active devices.

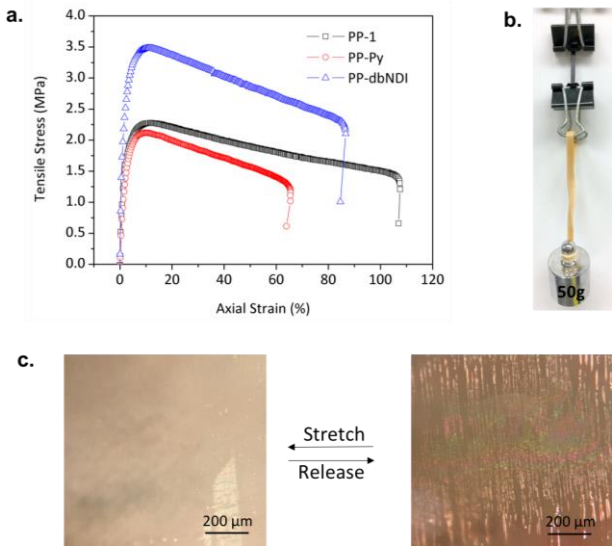

Fig. 4 Characterization of mechanical properties. (a) Tensile stress-strain curves of PP-1, PP-Py, and PP-dbNDI under a loading rate of 50 mm/min. (b) Constant stress test of 1 MPa applied to PP-1 film for 1 hour. (c) Stretchability test of PP-Py on PDMS substrate.

Additionally, PP polymers possess good stretchability. To demonstrate this, PP-Py was coated on a polydimethylsiloxane (PDMS) substrate. The substrate was then stretched to 100% strain and released ten times, followed by observation under an optical microscope. The optical images show that PP-Py can be stretched by 100% without cracking (**Fig. 4c**). Compared with the elongation (65%) in tensile stress-strain test (**Fig. 4a**), the improved elongation (100%) benefits from the existence of PDMS substrate which uniformly distributes stress. Wrinkles were, however, observed after releasing PP-Py from stretching, implying that PP-Py shows partially plastic deformation during this process, as would be expected by the prior tensile test results.

2.4 Self-Healing Properties of the Polymers

Even with optimal mechanical properties, cracking damage may still develop in self-healing polymers, especially over long-term use. Typically, the cracking of polymers originates from microscale or even nanoscale defects. To mimic this damage, an AFM tip was used to indent the surface of PP-1 and PENDI films, resulting in two hole-like damage features with diameters of around 500 nm, respectively (**Fig. 5**). The shape of the damaged area in PENDI is a triangular cone, similar in shape to the AFM tip. The height profile along the selected black line reveals that both holes have a depth around 60 nm and surrounding bumps with height around 50 nm. Interestingly, the damage hole in PP-1 was much wider and less defined than that in the PENDI film. Also, there is no distinct bump around the hole in PP-1. We attribute this difference to the crosslinking effect of triPy. Without triPy, brittle PENDI dissipates the indentation energy from the AFM tip by both cracking and extrusion of surface, forming a sharp hole and bump. After adding triPy, PP-1 is able to dissipate the indentation energy by reversibly disrupting the CT interactions instead. The non-covalently crosslinked supramolecular structure allows PP-1 to dissipate energy over a much larger area. Consequently, PP-1 demonstrates higher resistance to crack formation. The height profiles alone the linear area in the films were measured again after heat treatment at 40 °C for varying times. The damaged area of PENDI barely changed even after heat treatment for 6 h, showing no self-healing property. By contrast, after heat treatment only for 2 h, the depth of the hole in PP-1 film decreased from around 50 nm to 20 nm, demonstrating apparent self-healing property. Raising the heat treatment time to 6 h, only a slight trace of the damaged area with a depth of 6 nm was observed. We hypothesize that this self-healing effect of PP-1 film is due to the rebuilding of the CT interactions following breakage.

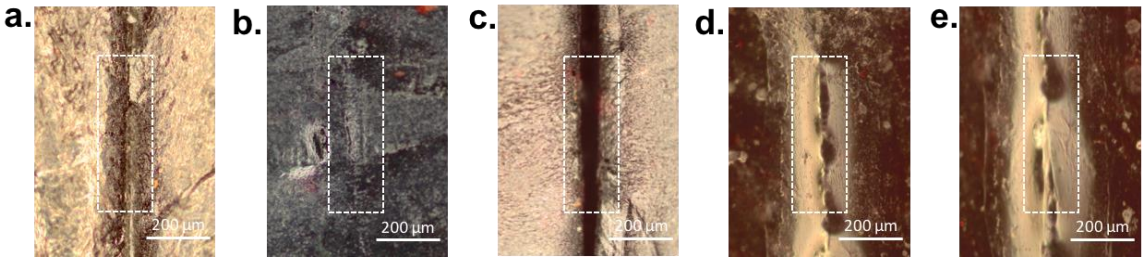

Fig. 6 Optical images of PP polymer films after cutting and heat treatment. (a) PP-dbNDI after heat treatment at 60 °C for 2 h. (b) PP-1 after heat treatment at 50 °C for 2 h. (c) PP-1 after heat treatment at 30 °C for 24 h. (d) PP-Py after heat treatment at 40 °C for 2 h. (e) PP-Py after heat treatment at 30 °C for 24 h.

To further investigate the effect of different binding modes between NDI and Py groups on self-healing properties, we conducted self-healing tests with bulk polymer films (**Fig. S9**). The polymer films were cut into two pieces and then lightly contacted together without additional pressure. Clear cuts with width of 20-200 μm were observed (**Fig. S10**). These broken films were heat treated at varying temperature for varying time, then observed by optical imaging. As shown in **Fig. 6**, PP-dbNDI displayed distinct self-healing properties after heat treatment at 60 °C for 2 h (**Fig. 6a**). The cut on PP-1, on the other hand, had almost disappeared after healing at 50 °C for 2 h (**Fig. 6b**). PP-1 was unable to heal at 30 °C, however, even after heat treatment for 24 h (**Fig. 6c**). PP-Py demonstrated significant healing after heat treatment at 40 °C for 2 h (**Fig. 6d**) and even at 30 °C for 24 h (**Fig. 6e**). We attribute the higher self-healing temperature of PP-dbNDI to its stronger binding mode, which requires more thermal energy to break reversible interactions. Although PP-1 and PP-Py possess the same binding mode, the lower self-healing temperature of PP-Py can be explained by its lower crosslinking density.

Therefore, despite sharing the same polymer components, their sensitivities to temperature are different. Based on this interesting feature, we fabricated a double-layer PP composite thin film by assembling and then pressing PP-Py and PP-dbNDI together (**Fig. 7a, Fig 7b**). As shown in **Fig. 7c** and **Movie S1** (Supporting Information), the double-layer thin film was first bended to the side of PP-dbNDI. Under heat treatment of 60 °C, the bended film gradually became straight and then automatically bended to the opposite side (the side of PP-Py) in 60 s. We attribute this bending shift to the much weaker 1:1 binding mode in PP-Py than that of 2:1 binding mode in PP-dbNDI: after fabricated by pressing, the polymer chains of the bulk films were stretched, leading to shrinkage stress within the films. Meanwhile, the polymer chains were reversibly crosslinked via pi-pi interactions, which locked the polymer chains and impeded their shrinkage. When the temperature went up to 60 °C, the reversible interactions began to break and rebuild much more quickly, leading to the unlocking and shrinkage of polymer chains. The much quicker shrinkage of PP-Py drives the composite films to bending to its side.

Uniaxial tensile tests were further conducted after cutting and healing the films to quantitatively investigate the self-healing efficiency of PP-1, PP-dbNDI, and PP-Py at different temperatures of 40, 50, and 60 °C (**Fig. S11**). The self-healing efficiency was estimated by the recovery of maximum tensile stress. As shown in **Fig. 8a**, even after heat treatment at 40 °C, all samples show self-healing efficiencies higher than 55%. Due to its weaker binding strength and lower crosslinking density, PP-Py possesses highest self-healing efficiency, which is higher than 85% even after heat treatment at 40 °C. **Fig. 8b** reveals that the all healed films still possess high Young's moduli (> 60 MPa), which helps increase the durability and lifetime

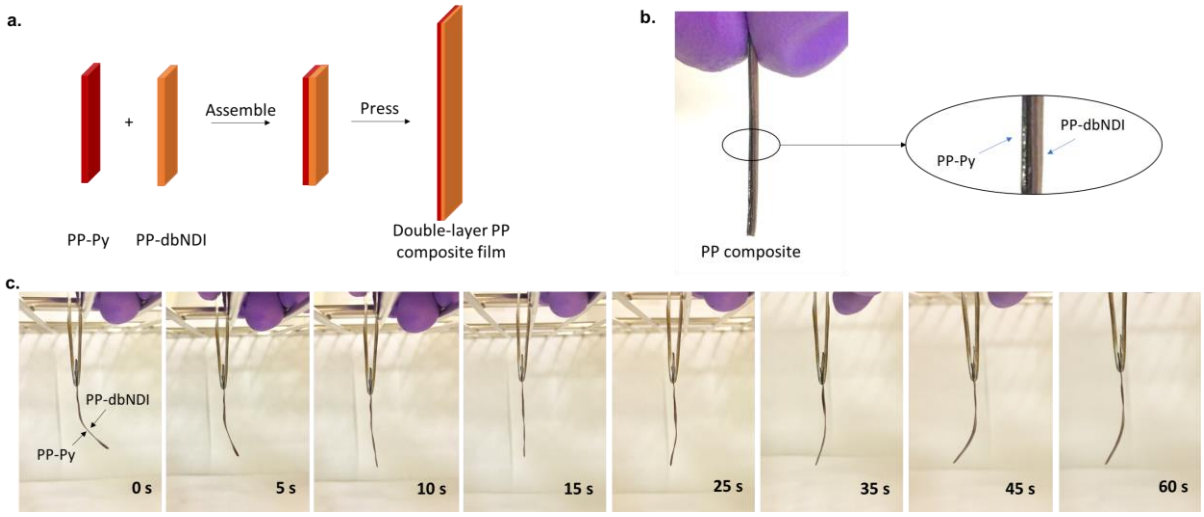

Fig. 7 (a) Schematic representation of the fabrication of double-layer PP composite film. (b) Optical images of the PP-Py/PP-dbNDI double-layer composite film. (c) The bending shift process of PP-Py/PP-dbNDI double-layer composite film under 60 °C.

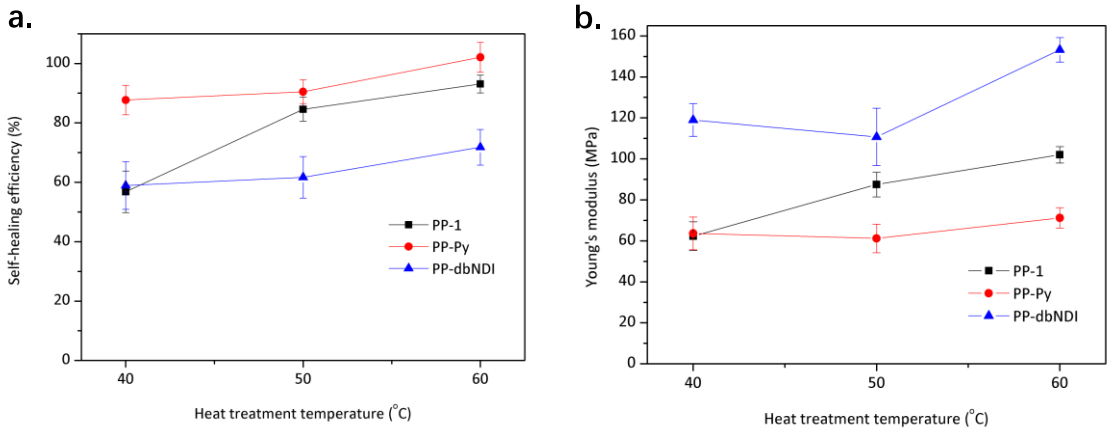

Fig. 8 The self-healing efficiency tests (a) and Young's moduli recovery (b) of PP polymer films after cutting and heat treatment at different temperature for 12 hours, respectively.

of materials. Note that since films were healed from a fully-broken state with no added pressure, air bubbles or inhomogeneous thicknesses may well have negatively impacted these results. Additional pressure during the test could definitely increase the self-healing efficiency due to the increase of contact area. The good thermal stability of both PENDI and triPy linker (**Fig. S4**) suggests that our polymer system could stand much higher temperature of heart treatment than 60 °C, which results in better self-healing efficiency.

Compared with previous reports (shown in **Fig. S12**), the polymer systems reported here not only possess very high Young's moduli (63-250 MPa), but also self-heal at relatively low temperatures (30-60 °C). Such a combination not only makes these materials suitable for devices in high-stress applications, but also allows these devices to enjoy self-healing benefits under mild thermal conditions.

2.5 Application in Lithium-Sulfur Battery

Besides tunable self-healing and mechanical properties, our design also displays great application potential in energy storage devices

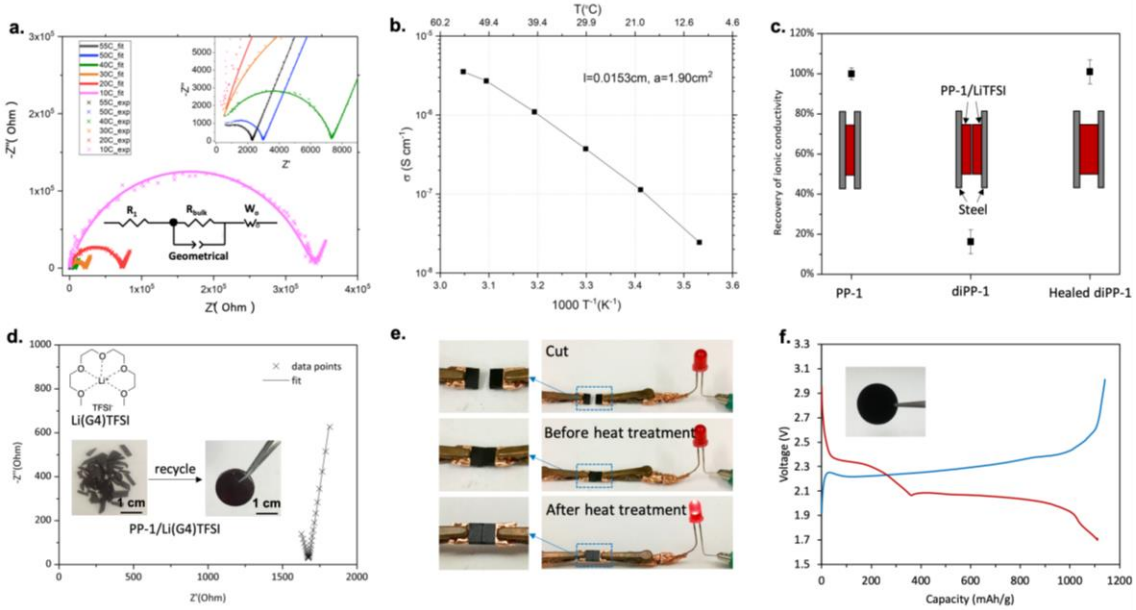

Fig. 9 (a) Nyquist plots and curve fits at different temperatures in electrochemical impedance spectroscopy tests of PP-1/LiTFSI. The inserted figure indicates the equivalent circuit to fit the plots: R_1 represents the entire internal resistance; R_{bulk} represents the bulk resistance of electrolyte; Geometrical represents the geometrical capacitance due to the presence of electrolyte with a finite dielectric constant between the two parallel metallic electrodes; W_o represents the resistance against the Warburg diffusion process of Li ion.[51,52] (b) Ionic conductivity of PP-1/LiTFSI at different temperatures. (c) Self-healing recovery test of PP-1/LiTFSI based on ionic conductivity. (d) Nyquist plots and curve fit of PP-1/Li(G4)TFSI at room temperature and recovery of PP-1/Li(G4)TFSI under 40 °C for 12 h (inside). (e) Recovery of composite film as electron conductive pathway in circuit. (f) Discharge/charge voltage profiles at 0.2C of sulfur cathode by using PP-1 as binder (sulfur loading 0.9 mg/cm^{-2}).

such as lithium-sulfur batteries. First, our polymers exhibit the ability to solvate and transport ions as a solid electrolyte, due to the prevalence of oligo(ethylene oxide) moieties in both PENDI and triPy. To demonstrate this, PP-1 supramolecular polymer was doped with salt LiTFSI and solvate ionic liquid (SIL), respectively. After doped with LiTFSI in a 20:1 [EO]:[Li^+] molar ratio, the resulting material PP-1/LiTFSI was sandwiched between stainless steel discs, followed by electrochemical impedance spectroscopy (**Fig. 9a**). Curve fitting the resulting Nyquist plot to a standard model for ion-conductive solids reveals the polymer system to have an ionic conductivity >10^{-6} S/cm at 50°C (**Fig 9b**), showcasing the application potential of this material as an electrode binder or solid-state electrolyte in batteries. Once cracking damage occurs, ionic conductivity in a solid electrolyte will decrease dramatically due to the disconnection of conductive pathways. We demonstrated this effect by sandwiching two individual PP-1 films between stainless steel discs for an ionic conductivity test. As shown in **Fig. 9c**, due to the existence of a physical gap between the films, the measured ionic conductivity of the stack is only about 16% that of a continuous film of PP-1. However, upon heating at 50 °C for 12 h, the physical disconnection was completely healed, resulting in 100% recovery of ionic conductivity. The Young's modulus increases to 132 MPa due to the interaction between Li ion and [EO] units. In order to improve the ionic conductivity further, PP-1 was doped with SIL Li(G4)TFSI (**Fig. 9d**). Due to their good compatibility, high doping amount of SIL was applied (33 wt.%). The resulting PP-1/Li(G4)TFSI exhibits high ionic conductivity of 1.01x10^{-5} S/cm even at room temperature, and reasonable Young's modulus (8 MPa, **Fig. S13**).

Besides, the polymer system possesses good compatibility with carbon and could function as cathode binder in lithium-sulfur battery. We made a freestanding composite film by uniformly dispersing sulfur/MJ430 mesoporous carbon composite (65 wt.%) and carbon black (5 wt.%) in PP-1 film (30 wt.%). Due to the high content of carbon, the resulting film demonstrated high electron conductivity by lighting light-emitting diode (LED) in the electrical circuit (**Fig. 9e**). The circuit was broken after we cut the composite film and even contacted the two pieces together. However, the LED could illuminate again after heating the broken composite film. This test not only implies the function of PP-1 as effective binder to integrate particles together, but also its self-healing property to recovery the electron conductive pathway. To investigate its effect in real cell, we made the sulfur cathode by dissolving the composite film into N-methyl-2-pyrrolidone and then casting on aluminum foil, followed by solvent evaporation. Consequently, a robust sulfur cathode was made and cycled at C/5 with lithium metal as anode. As shown in **Fig. 9f**, the cathode exhibits a high initial discharge capacity of 1109 mAh/g, with two typical discharge voltage plateaus at 2.30 and 2.06 V, respectively. This result shows promise for its use in future electrochemical devices.

3. Conclusions

In conclusion, we present an effective and feasible material design strategy to engineer the self-healing and mechanical properties of supramolecular polymers for diverse applications without requiring synthesis of new covalent structures. This design strategy was applied to produce a series of self-healing materials based on tunable non-covalent interactions between NDI and Py functionalities, and the resulting composites exhibit remarkable features: (1) high stiffness and good stretchability to help maintain physical integrity in devices; (2) widely tunable self-healing temperature and mechanical properties to satisfy various application requirements; (3) good ionic conductivity and high self-healing efficiency to provide durable ion-conductive pathways in potential electrochemical applications, especially energy storage area. Moreover, our strategy to decouple crosslinking properties from polymer structure is generally applicable, and we hope it will inspire the further engineering of improved supramolecular systems for effective integration of self-healing behavior into real devices. We plan to explore specific implementations of our materials design in future publications.

4. Experimental Section

4.1 Materials

All chemicals and reagents were purchased from Sigma–Aldrich. Solvents for chemical synthesis were purified by distillation. Other chemicals and reagents were used as received without purification.

4.2 Characterizations

The ^{1}H and ^{13}C NMR spectra were recorded on a Bruker AV500 spectrometer using $CDCl_3$ or d_6-DMSO as solvents. Mass spectrometry (MS) was performed on Bruker APEX III 47e Fourier Transform mass spectrometer. Thermogravimetric (TGA) analyses were conducted on a Shimadzu TGA-50 thermogravimetric analyzer under nitrogen at a heating rate of 10 °C/min. UV-Vis spectra were recorded on a Varian Cary 5000 UV-Vis-NIR Spectrophotometer. All samples used for UV-Vis tests were prepared with dichloromethane as solvent. DSC measurements were performed in a heat-cool-heat cycle (-40 to 220 °C, 10 °C/min; 220 to -40 °C, -10 °C/min; -40 to 220 °C, 10 °C/min). About 5 mg of sample was used for each test. A Bruker ICON AFM in contact mode was used to determine the Young's modulus of polymer films. AFM tips were calibrated with radius of around 10 nm, spring constant of around 0.4 N/m, and sensitivity of around 50 nm/V. OlymScope was used for optical image tests.

4.3 Synthesis of N-hexyl-1,4,5,8-naphthalenetetracarboxy-1,8-monoanhydride-4,5-monoimide (2)

As shown in **Scheme S1**, to a stirred suspension of **1** (5.72 g, 20.0 mmol) in DI water (300 mL) was dropwise added n-hexylamine (12.1 g, 120 mmol) through an addition funnel at 0 °C during which the solution turned clear. The reaction mixture was stirred overnight and slowly allowed to warm up to room temperature, then refluxed for 2 hours and again cooled to 0 °C followed by the addition of 10% $HCl_{(aq)}$ (100 mL). The precipitate was collected by filtration, and washed with water and ice-cold methanol, which was then refluxed in a mixture of $HCl_{(conc.)}$ (40 mL) and THF (20 mL). The suspension was again filtered, and the solid collected was washed consecutively with water, methanol and ice-cold acetone to afford **2** as a pale yellow solid (6.61 g, 94%). ^{1}H NMR (d_6-DMSO, 500 MHz) δ 8.67(m, 4H), 4.03 (t, J = 7.5 Hz, 2H), 1.65 (m, 2H), 1.29-1.36 (m, 6H), 0.87 (t, J = 7.5 Hz, 3H); ^{13}C NMR (d_6-DMSO, 125 MHz) δ 162.31, 158.66, 131.82, 130.39, 128.43, 127.08, 126.07, 123.67, 39.02, 30.93, 27.25, 26.15, 21.95,

13.89; HRMS (m/z, ESI) Calcd for $C_{20}H_{17}NO_5$ 351.1107, found 351.1116.

4.4 *Synthesis of N-hexyl-N'-(2-hydroxyethyl)-1,4,5,8-naphthalenetetracarboxydiimide (3)*

To a stirring suspension of **2** (5.27 g, 15.0 mmol) in ethanol (150 mL) was dropwise added ethanolamine (1.10 g, 18 mmol) through an addition funnel at room temperature. The reaction mixture was then refluxed and stirred overnight. The precipitate was collected by filtration and washed with ice-cold methanol to afford **3** as a pale yellow solid (5.44 g, 92%). ^{1}H NMR (d_6-DMSO, 500 MHz) δ 8.53 (m, 4H), 4.83 (t, *J* = 5 Hz, 2H), 4.13 (t, *J* = 5 Hz, 2H), 4.00 (t, *J* = 7.5 Hz, 2H), 3.64 (m, 2H), 1.63 (m, 2H), 1.30–1.36 (m, 6H), 0.87 (t, *J* = 7.5 Hz, 3H); ^{13}C NMR (d_6-DMSO, 125 MHz) 162.28, 162.15, 130.11, 130.08, 125.95, 125.84, 125.74, 57.56, 42.06, 30.68, 27.10, 25.93, 21.69, 13.58; HRMS (m/z, ESI, $[M+H]^+$) Calcd for $C_{22}H_{23}N_2O_5$ 395.1607, found 395.1618.

4.5 Synthesis of N-hexyl-N'-(2-[methacryloyl]ethyl)-1,4,5,8-naphthalene tetracarboxydiimide (4)

To a stirring suspension of **3** (5.52 g, 14.0 mmol) in a mixed solvent of THF (70 mL) and DCM (70 mL), with trace amount of 4-methoxyphenol, was added distilled Et_3N (1.56 g, 15.4 mmol) and then cooled to 0 °C, after which freshly distilled methacryloyl chloride (1.61 g, 15.4 mmol) was added dropwise. The reaction mixture was gently heated to 40 °C and stirred overnight. After cooling to room temperature, the mixture was poured into cold methanol. The precipitate was collected by filtration then washed with ice-cold methanol to afford **4** as a pale yellow solid (5.56 g, 85%). ^{1}H NMR ($CDCl_3$, 500 MHz) δ 8.74 (m, 4H), 6.02 (s, 1H), 5.51 (s, 1H), 4.57 (t, *J* = 5 Hz, 2H), 4.50 (t, *J* = 5 Hz, 2H), 4.18 (t, *J* = 6.5 Hz, 2H), 1.84 (s, 3H), 1.74 (m, 2H), 1.33–1.44 (m, 6H), 0.89 (t, *J* = 0.89, 3H); ^{13}C NMR ($CDCl_3$, 125 MHz)δ 167.18, 162.84, 162.70, 135.87, 130.91, 126.81, 126.29, 125.96, 61.75, 40.97, 39.47, 31.45, 27.98, 26.69, 22.50, 18.19, 14.00; HRMS (m/z, ESI, $[M+H]^+$) Calcd for $C_{26}H_{27}N_2O_6$ 463.1869, found 463.1876.

4.6 Synthesis of Poly(N-ethyl-N'-hexyl-1,4,5,8-naphthalenetetracarboxydiimidyl methacrylate-co-triethylene glycol methyl ether methacrylate) (PENDI)

To a mixture of **4** (647 mg, 1.4 mmol), triethylene glycol methyl ether methacrylate (139 mg, 0.6 mmol) and AIBN (4 mg, 1.2 mol%) in a sealed flask was added THF (3 mL). The reaction mixture was degassed through 3 freeze-pump-thaw cycles and heated under 70 °C for one day with vigorous stirring. After cooling to room temperature, the mixture was poured into cold methanol. The precipitate was collected by filtration and washed with methanol to afford PENDI-C_6 as a white solid (730 mg, 93%). ^{1}H NMR ($CDCl_3$, 500 MHz) δ 8.39 (b, 28H), 4.02 (b, 48H), 3.52(b, 30H), 3.31(b, 9H), 1.60(b, 34H), 1.30(b, 72H), 0.88(b, 21H); GPC (M_n = 102.4 KDa, PDI = 1.30).

4.7 Determination of Quadrupole-Quadrupole Charge Transfer (CT) Interaction Strength

As shown in **Fig. S3**, the association constant of 1:1 and 2:1 CT binding modes were estimated by the UV-Vis dilution method: the absorbance (A) of the characteristic peak is measured with varying concentration (c, 0.002-0.02 M) of the complexes. Based on the Beer-Lambert law, equation 1 shows the relationship between association constant (K_a), c, and A. By plotting data in **Fig. S3**, K_a can be calculated without requiring knowledge of constants $\in$ and l. Using this method, the complexation energy of these two complexes were determined to be -8.19 kJ/mol (1:1) and -16.49 kJ/mol (2:1), respectively.

$$\frac{c}{A} = \left(\frac{1}{K_a \in l}\right)^{0.5} \frac{1}{A^{0.5}} + \frac{1}{\in l} \qquad (1)$$

4.8 Self-Healing Tests

As shown in **Fig. S9**, PP-1, PP-dbNDI, and PP-Py were fabricated into films with a diameter of 1 cm and thickness of 0.1 cm. The polymer films were cut into two pieces and then contacted together without additional pressure. Then heat treatments for varying time at different temperature were conducted, followed by optical image tests.

4.9 Uniaxial Tensile Tests

PP polymer films were fabricated with the size of 0.04x0.4x5 cm. The uniaxial tensile tests were conducted using a LoadFrame (Instron-5585) at room temperature. The loading rate is 50 mm/min.

4.10 Assembly of Lithium-Sulfur Battery

Composite film was dissolved in N-methyl-2-pyrrolidone, followed by casting the resulting slurry on aluminum foil. After heat treatment at 50 °C for 12 hours under vacuum, sulfur cathode was fabricated. Then the cell was assembled by using lithium metal as anode and Celgard 2500 as separator. The electrolyte was prepared by dissolving 1M LiTFSI and 1 wt.% $LiNO_3$ in dioxolane/dimethoxyethane (1:1 v/v).

Conflicts of interest

There are no conflicts to declare.

Acknowledgements

This work is supported by the Department of Energy, Office of Energy Efficiency and Renewable Energy (EERE), under Award Number DE-EE0007791.

Notes and references

1 T. Someya, Z. Bao and G. G. Malliaras, *Nature*, 2016, **540**, 379–385.

2 B. C. K. Tee, C. Wang, R. Allen and Z. Bao, *Nat Nano*, 2012, **7**, 825–832.

3 Y. Cao, T. G. Morrissey, E. Acome, S. I. Allec, B. M. Wong, C. Keplinger and C. Wang, *Adv. Mater.*, 2017, **29**, 1605099.

4 C.-H. Li, C. Wang, C. Keplinger, J.-L. Zuo, L. Jin, Y. Sun, P. Zheng, Y. Cao, F. Lissel, C. Linder, X.-Z. You and Z. Bao, *Nat Chem*, 2016, **8**, 618–624.

5 X. Liu, G. Su, Q. Guo, C. Lu, T. Zhou, C. Zhou and X. Zhang, *Adv. Funct. Mater.*, 2018, **28**, 1706658.

6 S. Choi, T.-W. Kwon, A. Coskun and J. W. Choi, *Science*, 2017, **357**, 279–283.

7 Z. Wei Seh, W. Li, J. J. Cha, G. Zheng, Y. Yang, M. T. McDowell, P.-C. Hsu and Y. Cui, *Nat. Commun.*, 2013, **4**, 1331.

8 H. Wu, G. Chan, J. W. Choi, I. Ryu, Y. Yao, M. T. McDowell, S. W. Lee, A. Jackson, Y. Yang, L. Hu and Y. Cui, *Nat. Nanotechnol.*, 2012, **7**, 310–315.

9 M. Wu, X. Xiao, N. Vukmirovic, S. Xun, P. K. Das, X. Song, P. Olalde-Velasco, D. Wang, A. Z. Weber, L.-W. Wang, V. S. Battaglia, W. Yang and G. Liu, *J. Am. Chem. Soc.*, 2013, **135**, 12048–12056.

10 C. Wang, H. Wu, Z. Chen, M. T. McDowell, Y. Cui and Z. Bao, *Nat. Chem.*, 2013, **5**, 1042–1048.

11 J. M. Whiteley, P. Taynton, W. Zhang and S.-H. Lee, *Adv. Mater.*, 2015, **27**, 6922–6927.

12 H. Cheng, Y. Huang, Q. Cheng, G. Shi, L. Jiang and L. Qu, *Adv. Funct. Mater.*, 2017, **27**, 1703096.

13 Y. Rao, A. Chortos, R. Pfattner, F. Lissel, Y. Chiu, V. Feig, J. Xu, T. Kurosawa, X. Gu, C. Wang, M. He, J. W. Chung and Z. Bao, *J. Am. Chem. Soc.*, 2016, **138**, 6020–6027.

14 J. Y. Oh, S. Rondeau-Gagné, Y.-C. Chiu, A. Chortos, F. Lissel, G.-J. N. Wang, B. C. Schroeder, T. Kurosawa, J. Lopez, T. Katsumata, J. Xu, C. Zhu, X. Gu, W.-G. Bae, Y. Kim, L. Jin, J. W. Chung, J. B.-H. Tok and Z. Bao, *Nature*, 2016, **539**, 411–415.

15 A. Chortos, J. Liu and Z. Bao, *Nat Mater*, 2016, **15**, 937–950.

16 J. A. Neal, D. Mozhdehi and Z. Guan, *J. Am. Chem. Soc.*, 2015, **137**, 4846–4850.

17 P. Cordier, F. Tournilhac, C. Soulié-Ziakovic and L. Leibler, *Nature*, 2008, **451**, 977–980.

18 M. Nakahata, Y. Takashima, H. Yamaguchi and A. Harada, *Nat. Commun.*, 2011, **2**, 511.

19 H. Ur Rehman, Y. Chen, M. S. Hedenqvist, H. Li, W. Xue, Y. Guo, Y. Guo, H. Duan and H. Liu, *Adv. Funct. Mater.*, 2018, **28**, 1704109.

20 A. Faghihnejad, K. E. Feldman, J. Yu, M. V. Tirrell, J. N. Israelachvili, C. J. Hawker, E. J. Kramer and H. Zeng, *Adv. Funct. Mater.*, 2014, **24**, 2322–2333.

21 B. Zhou, D. He, J. Hu, Y. Ye, H. Peng, X. Zhou, X. Xie and Z. Xue, *J. Mater. Chem. A*, 2018, **6**, 11725–11733.

22 D. Kim, S. Hyun and S. M. Han, *J. Mater. Chem. A*, 2018, **6**, 11353–11361.

23 D. Yang, Y. Wang, Z. Li, Y. Xu, F. Cheng, P. Li and H. Li, *J. Mater. Chem. C*, 2018, **6**, 1153–1159.

24 D. Mozhdehi, S. Ayala, O. R. Cromwell and Z. Guan, *J. Am. Chem. Soc.*, 2014, **136**, 16128–16131.

25 O. R. Cromwell, J. Chung and Z. Guan, *J. Am. Chem. Soc.*, 2015, **137**, 6492–6495.

26 L. R. Hart, J. H. Hunter, N. A. Nguyen, J. L. Harries, B. W. Greenland, M. E. Mackay, H. M. Colquhoun and W. Hayes, *Polym. Chem.*, 2014, **5**, 3680–3688.

27 K. E. Feldman, M. J. Kade, E. W. Meijer, C. J. Hawker and E. J. Kramer, *Macromolecules*, 2009, **42**, 9072–9081.

28 J. Hentschel, A. M. Kushner, J. Ziller and Z. Guan, *Angew. Chemie Int. Ed.*, 2012, **51**, 10561–10565.

29 Y. Chen, A. M. Kushner, G. A. Williams and Z. Guan, *Nat Chem*, 2012, **4**, 467–472.

30 G. A. Williams, R. Ishige, O. R. Cromwell, J. Chung, A. Takahara and Z. Guan, *Adv. Mater.*, 2015, **27**, 3934–3941.

31 J. Fox, J. J. Wie, B. W. Greenland, S. Burattini, W. Hayes, H. M. Colquhoun, M. E. MacKay and S. J. Rowan, *J. Am. Chem. Soc.*, 2012, **134**, 5362–5368.

32 I. Kovalenko, B. Zdyrko, A. Magasinski, B. Hertzberg, Z. Milicev, R. Burtovyy, I. Luzinov and G. Yushin, *Science*, 2011, **334**, 75–9.

33 Y. Shi, X. Zhou and G. Yu, *Acc. Chem. Res.*, 2017, **50**, 2642–2652.

34 F. Carpi, S. Bauer and D. De Rossi, *Science (80-.).*, 2010, **330**, 1759–1761.

35 S. C. B. Mannsfeld, B. C. K. Tee, R. M. Stoltenberg, C. V. H. H. Chen, S. Barman, B. V. O. Muir, A. N. Sokolov, C. Reese and Z. Bao, *Nat Mater*, 2010, **9**, 859–864.

36 F. Leng, C. M. Tan and M. Pecht, *Sci. Rep.*, 2015, **5**, 12967.

37 T. M. Bandhauer, S. Garimella and T. F. Fuller, *J. Electrochem. Soc.*, 2011, **158**, R1–R25.

38 Y. Chen, B. Lu, Y. Chen and X. Feng, *Sci. Rep.*, 2015, **5**, 11505.

39 A. J. Bandodkar, W. Jia, C. Yardımcı, X. Wang, J. Ramirez and J. Wang, *Anal. Chem.*, 2015, **87**, 394–398.

40 S. C. Grindy, R. Learsch, D. Mozhdehi, J. Cheng, D. G. Barrett, Z. Guan, P. B. Messersmith and N. Holten-Andersen, *Nat Mater*, 2015, **14**, 1210–1216.

41 M.-Y. Yeh and H.-C. Lin, *Phys. Chem. Chem. Phys. Phys. Chem. Chem. Phys*, 2421, **16**, 24216–24222.

42 M. Al Kobaisi, S. V Bhosale, K. Latham, A. M. Raynor and S. V Bhosale, *Chem. Rev.*, 2016, **116**, 11685–11796.

43 C. R. Martinez and B. L. Iverson, *Chem. Sci.*, 2012, **3**, 2191–2201.

44 A. Das and S. Ghosh, *Angew. Chemie Int. Ed.*, 2014, **53**, 1092–1097.

45 M. B. Nielsen, J. O. Jeppesen, J. Laut, C. Lomholt, D. Damgaard, J. P. Jacobsen, J. Becher and J. F. Stoddart, *J. Org. Chem.*, 2001, **66**, 3559–3563.

46 B. W. Greenland, S. Burattini, W. Hayes and H. M. Colquhoun, *Tetrahedron*, 2008, **64**, 8346–8354.

47 B. K. Ahn, D. W. Lee, J. N. Israelachvili and J. H. Waite, *Nat. Mater.*, 2014, **13**, 867–872.

48 N. Roy, B. Bruchmann and J.-M. Lehn, *Chem. Soc. Rev.*, 2015, **44**, 3786–3807.

49 D. L. Taylor and M. in het Panhuis, *Adv. Mater.*, 2016, **28**, 9060–9093.

50 Z. Wei, J. H. Yang, Z. Q. Liu, F. Xu, J. X. Zhou, M. Zrínyi, Y. Osada and Y. M. Chen, *Adv. Funct. Mater.*, 2015, **25**, 1352–1359.

51 W. Liu, S. W. Lee, D. Lin, F. Shi, S. Wang, A. D. Sendek and Y. Cui, *Nat. Energy*, 2017, **2**, 17035.

52 G. Wang, Y. Lai, Z. Zhang, J. Li and Z. Zhang, *J. Mater. Chem. A*, 2015, **3**, 7139–7144.

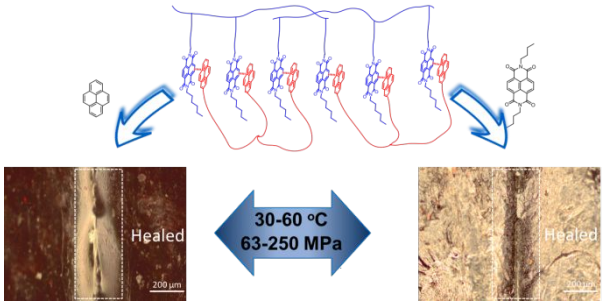

TOC

Stiff polymers with tunable self-healing and mechanical properties show promising potential in electrochemical devices